Hydrogen Redox in Protic Ionic Liquids and a Direct Measurement of Proton Thermodynamics

J. A. Bautista-Martinez,[†] L. Tang,[†] J.-P. Belieres,[‡] R. Zeller,[†] C. A. Angell,[‡] and C. Friesen*,[†]

School of Materials, and Department of Chemistry and Biochemistry, Arizona State University Tempe, Arizona 85287

Received: March 26, 2009; Revised Manuscript Received: May 4, 2009

Room temperature ionic liquids have attracted a great deal of interest in recent years due to their remarkable physicochemical properties including high thermal stability, wide electrochemical window, and low vapor pressure. A subclass of ionic liquids, protic ionic liquids (PILs), are formed by proton transfer from a Brønsted acid to a Brønsted base, and are good candidates as electrolytes in several applications, including fuel cells, because they integrate high ionicity and proton exchange kinetics with low vapor pressure. Here we present hydrogen redox results for a number of hydrogen-saturated PILs. Specifically we study the systems diethylmethylammonium bistrifluoromethanesulfonimide, diethylmethylammonium chloroaluminate, triethylammonium triflate, diethylmethylammonium triflate, dimethylethylammonium triflate, ethylammonium nitrate, pyridinium acetate, triethylammonium methane sulfonate, diethylmethylammonium methane sulfonate, and α-picolinium triflate. We observe a significant potential gap between the potential at which proton reduction occurs and the potential at which facile hydrogen oxidation occurs (with the gap ranging from ca. 0 to 800 mV). We show that this observation correlates with differences in the energetics for proton extraction from the anion (acid with the form HA) and from the cation (acid with the form BH^+), which is defined by the differences in proton free energy between the Brønsted couples HA/H^- and BH^+/B. This energy gap and the associated equivalence point in the titration curve fix the proton activity in these systems and determine the electrochemical potential needed to activate a proton when no lower energy sites are available in the vicinity of the electrode.

1. Introduction

Room temperature ionic liquids (RTILs) have diverse physicochemical properties including high thermal stability, wide electrochemical windows, negligible vapor pressure, and high ionic conductivity[1] which make RTILs attractive electrochemical solvents.[2,3] Because of this, RTILs are being explored in the electrochemical applications of solar cells,[4,5] fuel cells,[6,7] batteries,[8−10] and analytical electrochemical experiments.[11]

Much effort has been expended attempting to understand the electrochemical oxidation of hydrogen in RTILs[12] for the application in hydrogen fuel cells.[13,14] In general, RTILs are aprotic compounds without electrochemically available protons in their structures.[15] Alternatively, room temperature protic ionic liquids (PILs) are being considered as candidates for fuel cell electrolytes due to the advantage of having a defined proton activity as well as high proton conductivity, allowing for fuel cell operation under nonhumidified and high-temperature conditions.[1,16−20]

PILs are obtained by the transfer of a proton from an acid (HA) to a base (B) of a Brønsted acid−base pair, in contrast to RTILs where the species transferred is any group other than a proton. PILs often have higher conductivities and fluidities than the aprotic RTILs, as well as lower melting points as compared to the aprotic analogue.[13,19,20]

In this work, electrochemical hydrogen oxidation and proton reduction on polycrystalline platinum electrode surfaces is examined for ten PILs of widely varying proton transfer energies. We use the familiar electrochemical technique of cyclic voltammetry, in which the electrochemical potential at the Pt electrode immersed in a hydrogen-saturated PIL is swept at a fixed rate and the current density is monitored to give information on the different thermodynamic and kinetic processes that characterize the system.

We will show that a potential gap between the onset of hydrogen oxidation and proton reduction correlates surprisingly well with the proton transfer energetics associated with the formation of the PIL ($HA + B \rightarrow A^- + BH^+$) provided by aqueous solution pK_a data. We also examine the potential gap as a function of temperature, allowing for the direct extraction of enthalpic and entropic contributions to the proton transfer. A confirmation of the cyclic voltammetric behavior is made by using a twin hydrogen electrode cell that effectively provides the potentiometric titration curve of acid by base of which our PIL is the product.

The PILs studied comprise different combinations of the anions tetrachloroaluminate ($AlCl_4^-$), bis(trifluoromethylsulfonyl)imide ($(CF_3SO_2)_2N^-$, abbreviated TfSI) triflate ($CF_3SO_3^-$, Tf), methanesulfonate ($CH_3SO_3^-$, MS), nitrate NO_3^-, and acetate (CH_3COO^-, Ac) with the organic cations, triethylammonium (TEA), diethylmethylammonium (DEMA), dimethylethylammonium (DMEA), ethylammonium (EA), α-picolinium (Pic), and pyridinium (Py). We report on the combinations DEMATfSI, DEMA$AlCl_4$, TEATf, DEMATf, DMEATf, PicTf, TEAMS, DEMAMS, EAN, and PyAc.

1.1. Proton Energetics. The formation of a protic ionic liquid can be thought of in terms of proton donors and proton acceptors by using the framework developed by Gurney for aqueous

* To whom correspondence should be addressed.
[†] School of Materials.
[‡] Department of Chemistry and Biochemistry.

10.1021/jp902762c CCC: $40.75
Published on Web 06/11/2009

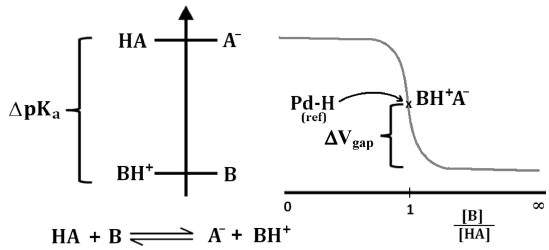

Figure 1. Reaction showing the formation of a protic ionic liquid and a representation of the energy gap across which the proton transfer occurs. The protic ionic liquid exists at the equivalence point of the acid−base titration curve; the abscissa corresponds to the ratio of titrated reactants.

solutions.[21,22] In this conception, a proton "falls" from an occupied energy level on the donor acid into the free acceptor level on the base to form a protonated cationic species. This reaction, which results in the protic ionic liquid, is represented in Figure 1.

Recognizing aqueous pK_a values as measures of proton affinity, and thus representative of the proton energy level, the free energy change of the reaction is related to the difference in pK_a between the Brønsted couples ($\Delta pK_a = pK_a^{BH^+/B} - pK_a^{HA/A^-}$). The relevance of p$K_a$ data to the thermodynamic properties of ionic liquids has previously been supported by an examination of the excess boiling point and potentiometric experiments.[22−25] The energetics of proton transfer are precisely provided by the actual pK_a values in the nonaqueous environment, and the general relevance of aqueous pK_a data to protic ionic liquids has heretofore been debatable. The equimolar reaction $HA + B \rightarrow A^- + BH^+$ and the associated ΔpK_a of the PIL thus formed provides for the Gibbs free energy of proton transfer $\Delta G = -2.303RT\Delta pK_a^{PIL}$. The Henderson−Hasselbalch equations for proton activity for acid-by-base and base-by-acid titration assuming unit activity are respectively

$$pH_{HA/A^-} = pK_a^{HA/A^-} + \log\frac{[A^-]}{[HA]} \quad \text{and} \quad pH_{BH^+/B} = pK_a^{BH^+/B} + \log\frac{[B]}{[BH^+]} \quad (1)$$

At the equivalence point (where the PIL exists), in the absence of solvent leveling effects the proton activity can be written

$$pH_{E.P.} = \frac{1}{2}(pH_{HA/A^-} + pH_{BH^+/B}) = \frac{1}{2}\left(pK_a^{HA/A^-} + pK_a^{BH^+/B} + \log\frac{[B][A^-]}{[BH^+][HA]}\right) \quad (2)$$

where the standard state is defined at the equivalence point for the PIL of interest. For perfectly equimolar mixtures, the last term in eq 2 goes to zero so that the proton activity at the equivalence point is simply

$$pH_{E.P.} = \frac{1}{2}(pK_a^{HA/A^-} + pK_a^{BH^+/B}) \quad (3)$$

With the proton activity known, the electrochemical potential for oxidation of hydrogen under saturated conditions in the PIL $A^- + {}^1/_2H_2 \rightarrow HA + 1e^-$ is given by

$$\Delta V_{E.P.} = -\frac{2.303RT}{F}pH_{E.P.} \quad (4)$$

and the potential for the reduction of protons $BH^+ + 1e^- \rightarrow B + {}^1/_2H_2$ is given by

$$\Delta V^{red} = -\frac{2.303RT}{F}pK_a^{BH^+/B} \quad (5)$$

where F is Faraday's constant, R is the gas constant, and T is the temperature. Thus, a potential "gap" is established between the potential at which hydrogen is oxidized (supported by protonation of A^-) and the potential at which protons are reduced (supported by deprotonation of BH^+)

$$\Delta V_{gap} = \Delta V_{E.P.} - \Delta V^{red} = \frac{2.303RT}{F}(pH_{E.P.} - pK_a^{BH^+/B}) = \frac{\Delta pK_a}{2}\frac{2.303RT}{F} \quad (6)$$

Equation 6 suggests an opportunity for directly extracting the proton transfer thermodynamics in PILs. Via the one assumption that PILs do not solvate bare protons, the potential gap between the facile hydrogen oxidation and proton reduction potentials provides the PIL ΔpK_a. In section 1.2 below we reintroduce these acid−base concepts for aqueous electrolytes.

1.2. Hydrogen Redox in Aqueous Electrolytes. Thus far, the discussion has focused on proton thermodynamics in equimolar protic ionic liquids. Understanding our current work is facilitated by recalling several key concepts in aqueous solution electrochemistry. In aqueous acid electrolytes, the proton carriers are hydronium ions generated by the addition of protic salts to water (e.g., $[H_3O^+][Tf^-]$). On an ideal electrode in the absence of specifically adsorbing or complexing ions, hydrogen redox is facile within millivolts on both sides of the reversible hydrogen electrode (RHE) supported by hydronium ions and dissolved hydrogen gas

$$\frac{1}{2}H_2 + H_2O \leftrightarrow H_3O^+ + e^- \quad (7)$$

In aqueous alkaline electrolytes, the proton carriers are hydroxyl ions, and again hydrogen redox is facile within a small potential of RHE, supported by hydroxyl ions and dissolved hydrogen gas

$$\frac{1}{2}H_2 + OH^- \leftrightarrow H_2O + e^- \quad (8)$$

However, it is important to recognize that in the absence of a protic salt, aqueous electrolytes made up of aprotic salts support minuscule rates of hydrogen reduction just negative of the hydrogen oxidation potential. This is because in the absence of protic salts the concentration of hydronium ions is of order 10^{-7} M. Therefore, while the hydrogen oxidation reaction is supported by the generation of H_3O^+, the reduction of the 10^{-7} M H_3O^+ just negative of RHE results in a diffusion limited current density that is very small. Significant reduction in neutral aqueous electrolytes only occurs at potentials negative enough to deprotonate H_2O to OH^-. The voltage difference, ΔV_{gap}, between the oxidation reaction eq 7 and facile reduction reaction

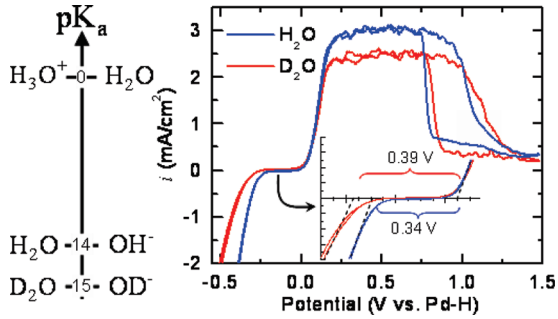

Figure 2. (Left) pK_a diagram for H_2O and D_2O. (Right) Voltammograms of activated Pt electrodes in aqueous hydrogen saturated 0.1 M $NaClO_4$ in (blue) H_2O and (red) D_2O. Scan rate 0.01 V s^{-1}.

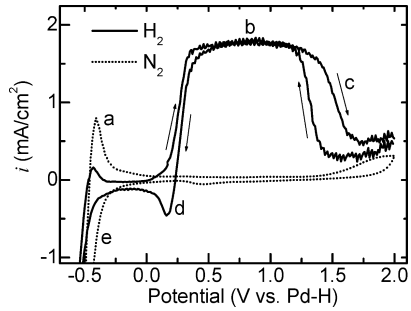

Figure 3. Voltammograms of activated Pt immersed in H_2-saturated TEATf (solid line) and N_2-saturated TEATf (dotted line). Scan rate 0.1 V s^{-1}.

eq 8 is given by eq 6, where the different conditions (i.e., different pH) at the upper and lower bounds of the gap identify eqs 7 and 8, respectively, to be the relevant reactions. Figure 2 displays a Gurney-type diagram for the pK_a values of H_2O and D_2O. In hydrogen saturated aqueous electrolytes of aprotic salts, eq 6 provides calculated values of $\Delta V_{gap} = 0.414$ V for H_2O and $\Delta V_{gap} = 0.444$ V for D_2O. Figure 2 also displays voltammograms for hydrogen-saturated $NaClO_4$ electrolytes of H_2O and D_2O. As is seen in the figure, hydrogen oxidation occurs at 50 mV vs. the Pd−H reference electrode (described in the next section). However, reduction in H_2O occurs only negative of −290 mV (a measured ΔV_{gap} of 340 mV) while reduction in D_2O occurs below −350 mV (a measured ΔV_{gap} of 390 mV), which provide experimental pK_a of 11.5 and 13.2, respectively (the actual values are 14 and 15, respectively). We have found that potentiodynamic measurements of ΔpK_a will generally tend to underestimate the calculated values by ca. 10% due to pH changes at the electrode−electrolyte interface during cycling.

1.3. Pd−H Reference Electrode and the Junction Potential. Ionic liquids are notorious for the sensitivity of their physicochemical properties to small quantities of water; a fact that makes it difficult to accurately measure their electrochemical behavior without contamination from an aqueous reference electrode. Nonaqueous reference electrodes, such as silver−silver chloride in acetonitrile, are common, but these still require the use of salt-bridges and porous frits to prevent contamination. Another more significant issue is the need to define the junction potential for each PIL chemistry studied, a tedious process if the interest is to elucidate general properties across a wide range of PIL systems. A solution to these challenges is found in the palladium−hydrogen system in the form of the Pd−H reference electrode. This electrode takes advantage of a broad two-phase region in the Pd−H phase diagram to ensure a constant hydrogen chemical potential within the electrode, which is typically stable for up to 24 h in aqueous systems.[26] The facile hydrogen redox

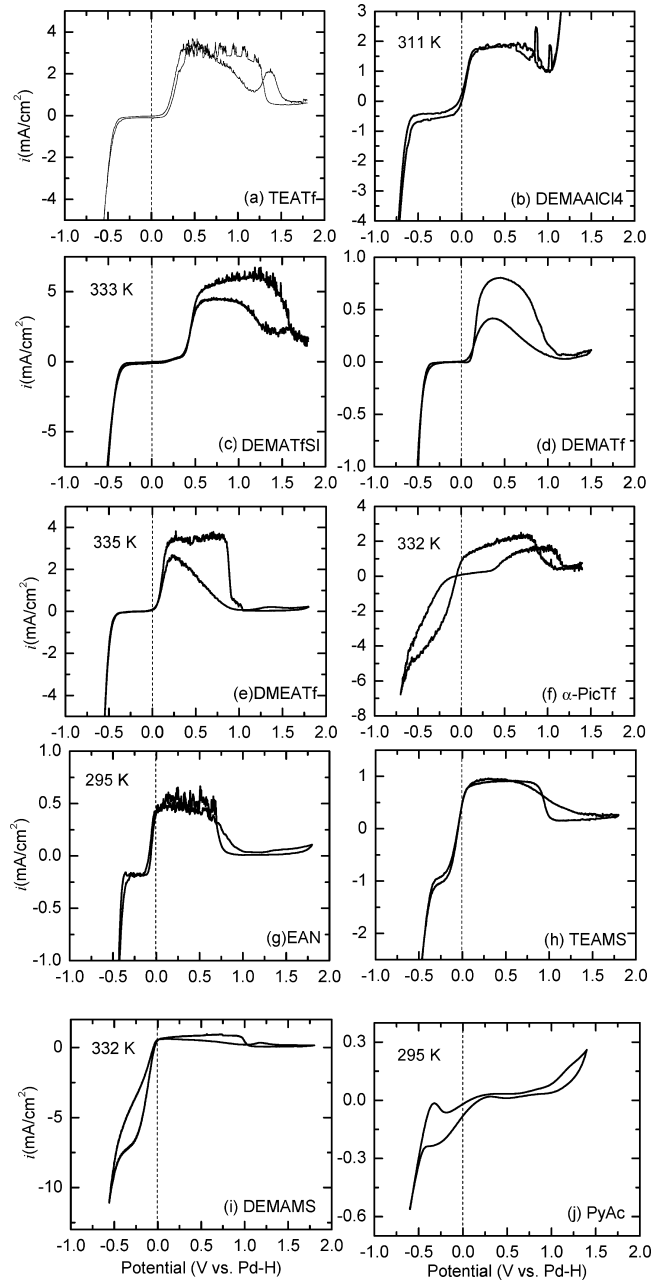

Figure 4. Voltammograms of activated Pt electrodes in hydrogen-saturated (a) TEATf, (b) $DEMAAlCl_4$, (c) DEMATfSI, (d) DEMATf, (e) DMEATf, (f) α-PiTf, (g) EAN, (h) TEAMS, (i) DEMAMS, and (j) PyAc. The potential gap is clearly visible around 0 V vs. Pd−H in all PILs (positive scan only in PicTf). Scan rate 0.01 V s^{-1}

at the palladium surface ensures that the electrode is always at or near the equilibrium potential. The use of Pd−H reference electrodes eliminates the issue of contamination from extraneous salts or solvents, addresses the junction potential, and provides a potential tied to the proton activity in the PIL.

The potential of the Pd−H electrode is defined by the hydrogen redox equilibrium at the palladium/electrolyte interface. In aqueous solutions the Pd−H potential is approximately 35 mV positive of the reversible hydrogen electrode, fixed by reversible proton promotion to the water molecule. In this work, we have found that the Pd−H electrode is the ideal reference electrode in PILs. This is because essentially all of the Brønsted bases are protonated, and in the absence of the ability to solvate a bare proton, the only state available in a PIL is on the anion of the original acid (i.e., its conjugate base, A^-), as shown

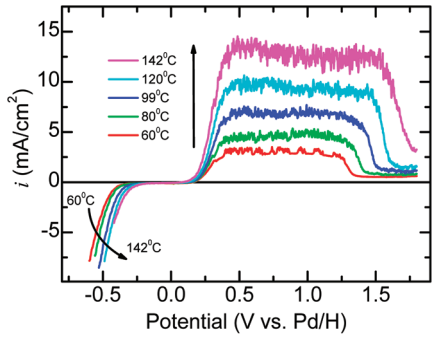

Figure 5. Voltammograms (negative branch only) of activated platinum immersed in H_2-saturated TEATf over a temperature range of 60 to 142 °C. Scan rate 0.1 V s^{-1}.

schematically in Figure 1. Accordingly, the potential to reform the original acid molecule is approximately 0 mV vs. the Pd−H reference electrode. It will be demonstrated in the data presented below that this concept to a large extent holds, though there is some scatter in the hydrogen oxidation potential.

2. Experimental Section

2.1. Materials. The PILs in this work were prepared by the stoichiometric addition of a Brønsted acid (HA) to a Brønsted base (B), either neat or in an aqueous solution, by the dropwise addition of the acid to an amine base, at low temperature. A few of the PILs, including DEMAAlCl$_4$, were prepared by metathetical reactions. Usually a small excess of base was added, and the PIL was then purified of the excess amine (and water in the aqueous case) by rotary evaporation at 80 °C (the partial pressure of amine always being greater than that of the acid near stoichiometry). A more detailed description of the synthesis of PILs is given in Belieres et al.[23] In the present work, Karl Fischer titration was used to confirm the elimination of water from the PILs since water must be minimized if we are to measure accurately the proton gaps of interest. Stoichiometry was confirmed by integration of the proton resonance peak in the 1H nuclear magnetic resonance spectrum for the N−H proton, and a sample was only accepted for further study if this integration yielded 1.00 protons and no free acid signal was detectable. Particularly for large proton gap PILs, the potential in the vicinity of stoichiometry is very sensitive to departures from stoichiometry, as will be seen below.

2.2. Electrochemical Measurements. Cyclic voltammetry was performed by using a conventional three-electrode sealed cell controlled by either a Gamry Potentiostat (Gamry Instruments, USA) or an Epsilon Potentiostat (BAS, USA). The platinum working and counter electrodes were cleaned in hot fuming HNO_3 followed by hot 18.1 M H_2SO_4 before being rinsed in 18.3 MΩ·cm water and hydrogen flame annealed. The Pd−H reference electrode was prepared according to the procedure outlined in ref 26.

The electrolyte media were stored in a nitrogen atmosphere. Prior to measurement a 3 mL sample was saturated with hydrogen (99.9999%) or nitrogen (99.9999%, both from Liquid Air America Corp, USA), by direct bubbling for at least 20 min. Complete saturation was verified by the stability of the open circuit potential values. At the beginning of an experiment, the PILs initially contained less than 100 ppm water. The postexperiment water concentration never exceeded 300 ppm.

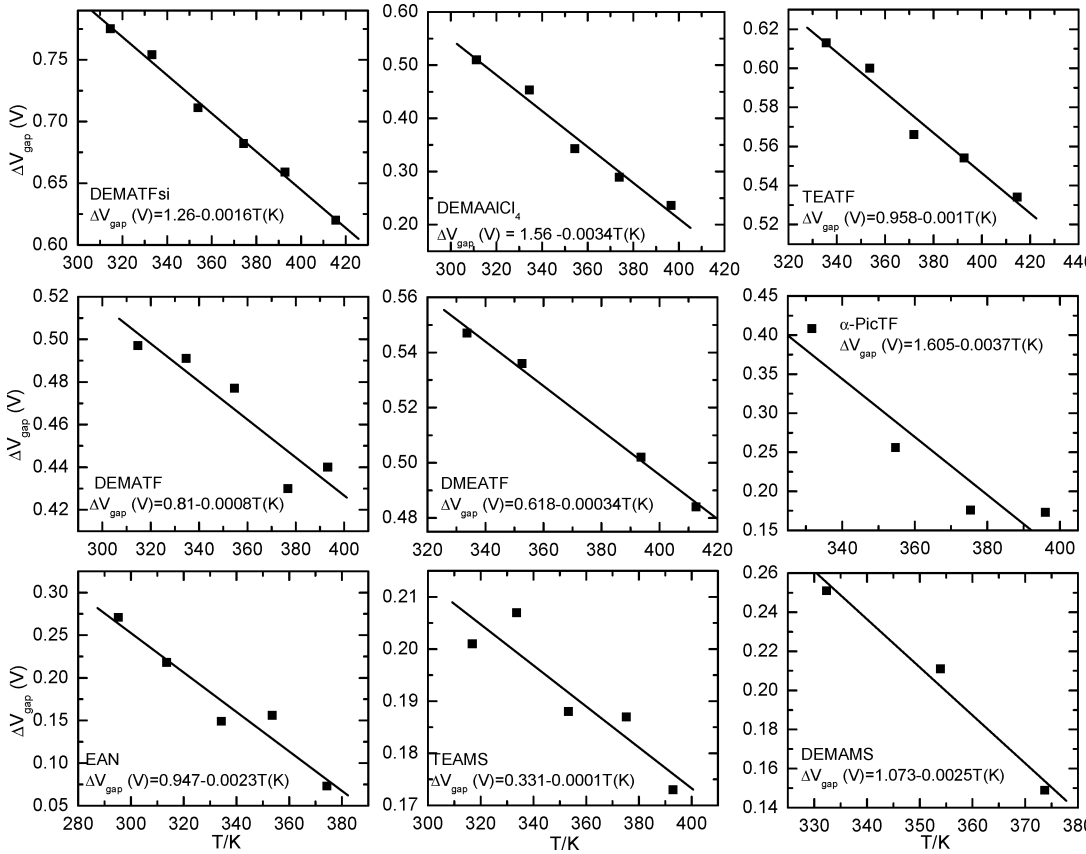

Figure 6. Variation of potential gap with temperature for (a) DEMATfSI, (b) DEMAAlCl$_4$, (c) TEATf, (d) DEMATf, (e) DMEATf, (f) α-PicTf, (g) EAN, (h) TEAMS, and (i) DEMAMS.

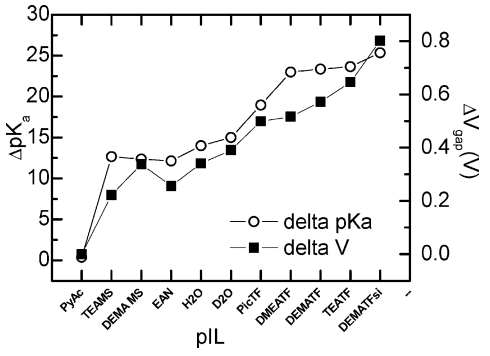

Figure 7. ΔpK_a (left ordinate) and ΔV_{gap} (right ordinate) plotted versus PIL, plotted in order of increasing ΔpK_a. All values extrapolated to 25 °C.

3. Results

3.1. Triethylammonium Triflate (TEATf) Example Case. For the purposes of introducing the general results, we take TEATf in which the proton gap is large (large ΔpK_a) and the results are particularly clearly defined. Figure 3 shows the behavior of TEATf under cyclic voltammetry at 60 °C between −0.6 and +2.0 V vs. Pd−H on an activated platinum electrode. Under hydrogen-saturated conditions, the onset of hydrogen oxidation (labeled "b" in Figure 3) was observed in the positive scan between ca. 0.0 and 1.6 V (see the Supporting Information for a discussion on Pt electrode activation). This signal decreased quickly above 1.4 V (Figure 3, curve c), where a Pt oxidation wave is observed in the nitrogen-saturated case, and in the negative scan, the hydrogen oxidation wave was again observed below 1.3 V. Platinum oxides have been shown to inhibit hydrogen oxidation in aqueous solutions[27,28] and in aprotic ionic liquids due to traces of water.[23] In PILs, however, the electrochemical oxidation of platinum in the presence of triflate ions could produce platinum(II) triflate complexes, which are a stable species synthesized in nonelectrochemical experiments.[29] In both the positive and negative scan directions, the diffusion-limited current density for oxidation was ca. 1.8 mA/cm^2. Continuing in the negative direction, at approximately 0.3 V the current decreased rapidly followed by a reduction wave (Figure 3, curve d). Under both hydrogen and nitrogen saturated conditions a sustained reduction signal is observed negative of ca. −0.4 V (Figure 3, curve e) followed by a short-lived oxidation wave (Figure 3, curve a) upon cycling in the positive direction.

3.2. Hydrogen Redox in DEMATfSI, DEMAAlCl$_4$, TEATf, DEMATf, DMEATf, α-PiTf, EAN, TEAMS, DEMAMS, and PyAc. Figure 4 displays cyclic voltammograms for ten different hydrogen-saturated PILs. All the data shown in Figure 4 were recorded while actively bubbling hydrogen gas over an activated platinum electrode. The five regions identified in reference to Figure 3 are seen in each of the PILs. Per the principles described in Section 1.3, the onset potential for sustained hydrogen oxidation is defined by ca. 0 mV vs. Pd−H. As seen in Figure 4, the Tafel regime for hydrogen oxidation starts *near* 0 mV, but due to the dynamic nature of the measurement, which results in proton activity changes local to the electrode and overpotential differences, the actual hydrogen oxidation potentials are scattered about the reference potential: DEMATfSI (79 mV), DEMAAlCl$_4$ (−110 mV), TEATf (9 mV), DEMATf (−31 mV), DMEATf (−67 mV), α-PicTf (−178 mV), EAN (−153 mV), TEAMS (−223 mV), DEMAMS (−275 mV), and PyAc (no-gap). Another artifact of the potentiodynamic measurement is that the region within ΔV_{gap} often corresponds to a cathodic current, instead of a zero-current regime. This is due to passing

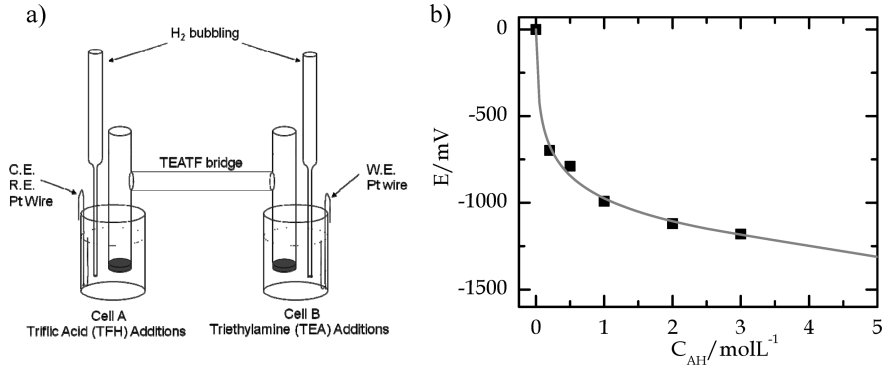

Figure 8. (a) Bridge cell arrangement for OCP titration experiments; cell A and cell B contain solutions of varying quantities of acid and base in TEATf, respectively. (b) Plot of open circuit potential with respect to the molar concentration of the acid or base.

TABLE 1: Experimental (at 298.15 K) and Calculated[a] Electrochemical Gaps of the Different PILs Studied in This Work

system	$\Delta V_{gap\text{-}pred}$, V	$\Delta V_{gap\text{-}exp}$, V	eq. point, V	ΔpK_a(aq)	ΔpK_a(exp.)	Δ, %
DEMATfsi	0.750	0.802	−0.139	25.35	27.1	6.9
TEATf	0.700	0.646	−0.069	23.65	21.8	−7.8
TEATf[b]	0.700	0.616[b]	−0.069	23.65	20.8[1]	−12.0
DEMATf	0.691	0.572	−0.080	23.35	19.3	−17.3
DMEATf	0.680	0.516	−0.089	22.99	17.4	−24.3
α-PicTf	0.561	0.499	−0.207	18.96	16.8	−11.4
DEMAMS	0.365	0.338	0.245	12.35	11.4	−7.7
EAN	0.359	0.256	0.276	12.13	8.6	−29.1
TEAMS	0.374	0.222	0.255	12.65	7.5	−40.7
PyAc	0.011	0	0.426	0.36	0	
H_3O^+/H_2O	0.414	0.341	0.414	13.99	11.5	−17.8
D_3O/D_2O	0.444	0.391	0.443	14.99	13.2	−11.9
DEMAAlCl4	—[c]	0.555	—[c]	—[c]	18.7	

[a] From eq 6. [b] Values obtained from the OCP experiments. [c] No literature data available for the $AlCl_4H$ pK_a.

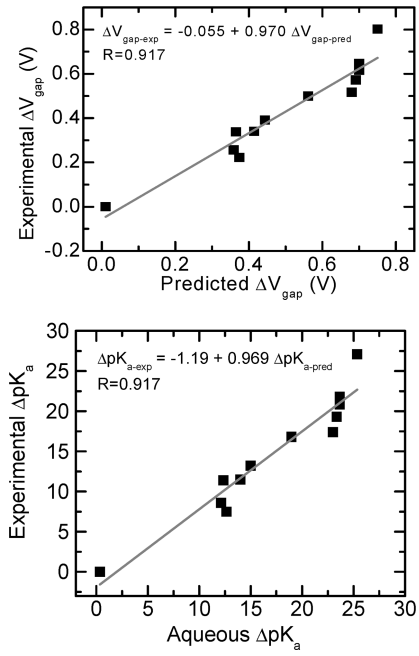

Figure 9. (Top) Plot of the experimentally determined ΔV_{gap} versus those predicted by eq 6. (Bottom) Plot of the experimentally determined ΔpK_a versus aqueous ΔpK_a data. All values are at 25 °C.

significantly more charge in the hydrogen oxidation part of the cycle (region b, Figure 3) than during the reduction reaction (region e, Figure 3), resulting in an excess of protonated acid that is then consumed under diffusion-limited conditions at potentials negative of region b in Figure 3.

In all systems except PyAc, the proton reduction reaction initiates at significantly more negative potentials than the hydrogen oxidation reaction. The range of the hydrogen oxidation window is limited on the positive end by the onset of platinum oxidation. Except in the case of PicTf, there exists a well-defined potential gap between facile hydrogen oxidation on the positive end and facile proton reduction on the negative end (this gap only appears on the positive scan in PicTf).

Figure 5 shows a series of voltammograms in hydrogen-saturated TEATf over a range of temperatures. The gap between the oxidation wave and the reduction wave decreases dramatically as temperature increases. Also, due primarily to increased fluidity of the TEATf, the diffusion-limited current density for hydrogen oxidation increases from 3.1 mA/cm^2 at 60 °C to 13.5 mA/cm^2 at 142 °C, a factor of ca. 4.4. This increase correlates well with the observed increase in fluidity by ca. 3.5 times for the same temperature change.[23] The temperature dependence of the hydrogen redox potential gap was examined, as shown in Figure 6. All systems show a temperature-linear behavior and the slopes for each of the systems are as follows: TEATf, −1.03 mV/K; DEMATf, −0.803 mV/K; DMEATf, −0.342 mV/K; PicTf, −3.71 mV/K; EAN, −2.31 mV/K; TEAMS, −0.103 mV/K; DEMATfSI, −1.55 mV/K; DEMAAlCl$_4$, −3.38 mV/K; and DEMAMS, −2.46 mV/K. These measurements allow for the comparison of PILs with a wide range of melting point by extrapolating ΔV_{gap} to 25 °C.

Figure 7 is a plot of the ΔpK_a values taken from aqueous data and the measured ΔV_{gap} plotted as a function of the PIL system extrapolated to 25 °C. Note the strong correlation.

In addition to voltammetric determination of ΔV_{gap}, a bridge cell arrangement was used to characterize the titration response of TEATf under hydrogen-saturated conditions, as shown schematically in Figure 8a. The salt bridge in this setup is composed of neat TEATf to minimize the junction potential. Equal quantities of acid (TfH) and base (triethylammonia, TEA) were titrated into their respective cells and the open-circuit potential was recorded as a function of the excess reagent. As seen in Figure 8b, the titration experiment results in a Nernstian response in potential. Extrapolating the response to the molar volume of TEATf (4.9 M), it is straightforward through eq 1 to extract the ΔpK_a for TEATf from this experiment, $\Delta V_{gap} = 0.616 \rightarrow \Delta pK_a = 20.8$, which corresponds well to the aqueous value of $\Delta pK_a = 24.7$. The autodissociation constant (pK_i) of TEATf (TEATf $\leftrightarrow$ TEA$^+$ + Tf$^-$) may also be approximated at 1 M excess acid and base, $pK_i \approx 16.51$.

The equivalence point in a series of calculated titration curves (see the Supporting Information) was used to compute a predicted $\Delta pK_{E.P.}$ and ΔV_{gap}. Table 1 displays both predicted and experimental ΔV_{gap} for all of the PILs in this work. Additionally, we show experimental ΔpK_a numbers derived from ΔV_{gap}.

4. Discussion

In nitrogen-saturated PILs, such as in Figure 3, the conjugate acid (BH$^+$) is reduced at (e) to release hydrogen gas according to the reaction

$$BH^+ + e^- \rightarrow B + \frac{1}{2}H_2 \qquad (9)$$

The potential at which this occurs is indicative of the relative strength of the Brønsted base, as it is related to the energy required to strip the proton from the conjugate acid. At reaction a in Figure 3 the deprotonated base generated during reaction e in Figure 3 that remains local to the electrode is reprotonated by the oxidation of dissolved hydrogen.

$$B_{local} + \frac{1}{2}H_2 \rightarrow BH^+ + e^- \qquad (10)$$

The charge observed under this short-lived wave increases with increasing time held negative of the reduction potential and is muted during rotating disk electrode (RDE) experiments (see the Supporting Information). The muting of reaction a in Figure 3 during an RDE experiment is due to the forced convection of deprotonated base B away from the electrode−electrolyte interface during reduction, significantly decreasing the presence of this species for reprotonation upon cycling in the positive direction.

In hydrogen-saturated PILs, oxidation is supported positive of ca. 0 V vs. Pd−H, as seen in region b of Figure 3 and all of the CVs of Figure 4. At these potentials, hydrogen oxidation is supported by the reprotonation of the conjugate base A$^-$.

$$A^- + \frac{1}{2}H_2 \rightarrow HA + e^- \qquad (11)$$

The reduction wave, Figure 3d, corresponds to the deprotonation of the HA present at the interface after cycling to more positive potentials.

$$HA_{local} + e^- \rightarrow A^- + \frac{1}{2}H_2 \qquad (12)$$

The charge associated with wave d is substantially smaller than that of the oxidation wave b, and is eliminated in rotating disk electrode experiments, as described for the excess conjugate base, B, generated during reaction 9.

The potential difference between reactions 9 and 11 is associated with the differences in Gurney-type energetics of the couples HA/A^- and BH^+/B, and consequently must be related to the differences in pK_a (ΔpK_a) between the couples. Heretofore, there existed limited evidence that aqueous pK_a data were generally appropriate in describing proton transfer energetics in PILs. Comparison of various PILs (Figure 7 and Table 1) reveals that the potential gap ΔV_{gap} for hydrogen redox and the approximation of ΔpK_a through eq 6 are *strongly correlated* to aqueous pK_a data for the systems studied here. Figure 9 shows a plot of the experimental potential gap versus the potential gap calculated from aqueous ΔpK_a data for all of the PILs studied, and a plot of the ΔpK_a extracted from the experiment versus aqueous pK_a data. These correlation plots have slopes within 3% of unity, with a ΔpK_a intercept offset of ca. -1.2.

From the data shown in Figure 6, it is straightforward to extract the thermodynamics of the proton transfer reaction $HA + B \rightarrow A^- + BH^+$, as shown in Table 2. Interestingly, there is little correlation between the entropic contribution to proton transfer and the PIL composition. The four PILs comprised of $DEMA^+$ cations span from a ΔS of 0.085 to 0.326 kJ/(mol·K), a factor of almost 4. The four PILs comprised of Tf^- anions range from 0.077 to 0.358 kJ/(mol·K), a factor of more than 4.6. This result is a bit surprising in the sense that the strong correlation between aqueous pK_a and our extracted pK_a data suggests that electrostatic interactions dominate. However, the lack of trends in the entropic contributions to proton transfer thermodynamics across the ion pairs studied suggests that the details of the chemistries involved have a significant impact.

Passing Faradaic current during the experiments performed in this work likely has a significant impact on the structure of the PILs. The removal of the PIL cations (anions) during reaction 9 (reaction 11) at the electrode−electrolyte interface disrupts local charge neutrality. This disruption almost certainly leads to the rejection of the conjugate ion from the interface: A^- during the reduction reaction in reaction 9 and BH^+ during the oxidation reaction in reaction 11. Additionally, the deprotonated base B produced during the reduction reaction and the protonated acid AH generated during the oxidation reaction should enhance proton transport through proton exchange reactions between B/BH^+ and AH/A^- conjugate species. Large length scale (ca. 25 Å) charge oscillations have been shown to exist in neat ionic liquids.[30] The disruption of local charge balance during redox processes involving the PILs and the rejection of the conjugate PIL ions from the interface likely generate something of an "extended" double-layer structure. During hydrogen redox in PILs, it is clear that the complexity of this charge-compensating and charge-screening structure[31,32] increases in intricacy. A significant opportunity for future research exists in developing a complete understanding of these phenomena.

TABLE 2: Thermodynamic Data for PILs As Derived from ΔV_{gap} vs. T

PIL	ΔG at 25 °C, kJ/mol	ΔH, kJ/mol	ΔS, kJ/(mol·K)
DEMATfsi	−77.70	−33.57	0.148
DEMAAlCl4	−53.59	43.60	0.326
TEATf	−62.83	−33.31	0.099
DEMATf	−49.92	−24.57	0.085
DMEATf	−55.72	−32.76	0.077
PicTf	−48.15	58.58	0.358
EAN	−24.78	41.70	0.223
TEAMS	−20.60	−9.56	0.037
DEMAMS	−32.74	37.92	0.237

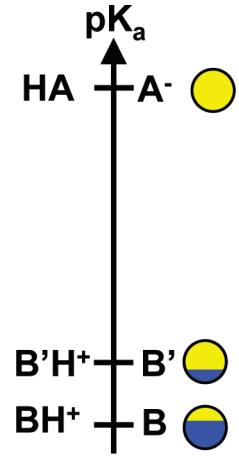

Figure 10. Gurney diagram representing a doping concept for enhancing Grotthuss-type proton conduction in PILs. The circles to the right represent proton occupancy: blue, occupied; yellow, unoccupied.

Finally, protic ionic liquids are now being explored as fuel cell electrolytes.[12,19,20] In a neat PIL, the proton carriers are, by necessity, HA species generated at the anode and consumed at the cathode. However, as is suggested by the data in Figure 3, the addition of excess base (B) to the ionic liquid allows for the sustained oxidation of hydrogen at significantly more negative potentials, where the proton carriers under those conditions are BH^+ species.

The point that the addition of excess base could improve the electrochemical performance of PILs suggests yet another concept for enhancing the Grotthuss-type characteristics of proton conduction in PILs. In colloquial analogy with doping semiconductors to generate defect levels that result in extrinsic electron−hole pairs, the addition of a base (B′) with a slightly smaller pK_a than the PIL base (B) should result in the thermal promotion of protons to the B′ level, as shown schematically in Figure 10. To the right of the Gurney-type diagram of Figure 10, the proton occupancy is represented in blue and the lack of occupancy is represented in yellow. An equilibrium population of proton-promoted/proton-vacant states should enhance vehicular transport both by providing a transition state and by enhancing the activity of the unoccupied B level. Such an electrolyte should exhibit significantly enhanced proton conductivity over a neat PIL.

5.0. Summary

Hydrogen redox was studied in ten protic ionic liquids, DEMATfSI, $DEMAAlCl_4$, TEATf, DEMATf, DMETf, PicTf, TEAMS, DEMAMS, EAN, and PyAc. Once activated, polycrystalline platinum electrodes exhibited a wide hydrogen oxidation wave, supported by the protonation of the species A^-. In most of the PILs, sustained proton reduction was only observed at potentials negative enough to deprotonate the species BH^+. The potential difference between these two processes is directly related to the pK_a difference of the Brønsted acid−Brønsted base pair that form the PIL. This PIL-specific ΔpK_a was extracted directly from our electrochemical experiments and compared to aqueous ΔpK_a data. A correlation plot between the current work and aqueous data gave a correlation slope

within 3% of unity, showing that aqueous pK_a data provide a good approximation to proton activity in PILs. Thus, the data provided in the proton free energy level diagrams (Gurney diagrams) of ref 23 should be almost quantitative, rather than qualitative as previously supposed, and should serve as a good basis for prediction of PIL properties.

Acknowledgment. This work was supported through the Center for Renewable Energy Electrochemistry, a state funded center, which is codirected by CF and CAA. The center is part of a larger effort: the Arizona Institute for Renewable Energy headed by Stephen Goodnick; we thank him for his efforts. The authors thank Dan Buttry and Karl Sieradzki for careful reads of the manuscript and their meaningful input. J.-P. B. was supported by DOD-ARO under grant no. W911NF-04-1-0060.

Supporting Information Available: Experimental details; voltammograms for hydrogen oxidation in TEATf on a Pt electrode (Figure S1), RDE voltammograms of activated platinum immersed in Ar saturated TEATF (Figure S2) and in H_2-saturated TEATF at different rotation rates (Figure S3), calculated titration curves for the pILs (Figures S4 and S5), example of the V_{gap} obtained from the cyclic voltammograms for the hydrogen oxidation in pILs (Figure S6), and voltammograms (cathodic branch only) of activated platinum immersed in H_2 saturated DEMATFsi, DEMAAlCl$_4$, TEATF, DEMATF, DMEATF, α-PicTF, EAN, DEMAMS, and TEAMS (Figure S7). This material is available free of charge via the Internet at http://pubs.acs.org.

References and Notes

(1) Yoshizawa, M.; Belieres, J. P.; Xu, W.; Angell, C. A. *Abstracts of Papers of the 226 Meeting of the American Chemical Society*; American Chemical Society: Washington, DC, 2003; U627.

(2) Adam, D. *Nature* **2000**, *407*, 938.

(3) Endres, F.; Sein El Abedin, S. *Phys. Chem. Chem. Phys.* **2006**, *18*, 2101.

(4) Santa-Nokki, H.; Busi, S.; Kallioinen, J.; Lahtinen, M.; Korppi-Tommola, J. J. *Photochem. Photobiol. A: Chemistry* **2007**, *186*, 29.

(5) Kawano, R.; Matsui, H.; Matsuyama, C.; Sato, A.; Abu Bin Hasan Susan, Md.; Tanabe, N.; Watanabe, M. *J. Photochem. Photobiol. A* **2004**, *164*, 87.

(6) Xue, X.; Liu, C.; Lu, T.; Xing, W. *Fuel Cells 06* **2006**, *5*, 347.

(7) de Souza, R. F.; Padilha, J. C.; Gonçalves, R. S.; Dupont, J. *Electrochem. Commun.* **2003**, *5*, 728.

(8) Galiñski, M.; Lewandowski, A.; Stêpniak, I. *Electrochim. Acta* **2006**, *51*, 5567.

(9) Hu, Y.; Li, H.; Huang, X.; Chen, L. *Electrochem. Commun.* **2004**, *6*, 28.

(10) Fung, Y. S.; Zhou, R. Q. *J. Power Sources* **1999**, *81*−*82*, 891.

(11) Mihkel, K. *Crit. Rev. Anal. Chem.* **2005**, *35*, 177.

(12) Noda, A.; Susan, Md. A. B. H.; Kudo, K.; Mitsushima, S.; Hayamizu, K.; Watanabe, M. *J. Phys. Chem. B* **2003**, *107*, 4024.

(13) Xu, W.; Angell, C. A. *Science* **2003**, *302*, 422.

(14) Susan, M. A. B. H.; Noda, A.; Mitsushima, S.; Watanabe, M. *Chem. Commun.* **2003**, *8*, 938.

(15) Nakamoto, H.; Noda, A.; Hayamizu, K.; Hayashi, S.; Hamaguchi, H.-o.; Watanabe, M. *J. Phys. Chem. C* **2007**, *111*, 1541.

(16) Noda, A.; Susan, Md. A. B. H.; Kudo, K.; Mitsushima, S.; Hayamizu, K.; Watanabe, M. *J. Phys. Chem. B* **2003**, *107*, 4024.

(17) Matsuoka, H.; Nakamoto, H.; Susan, Md. A. B. H.; Watanabe, M. *Electrochim. Acta* **2005**, *50*, 4015.

(18) Susan, Md. A. B. H.; Yoo, M.; Nakamoto, H.; Watanabe, M. *Chem. Lett.* **2003**, *32*, 836.

(19) Susan, Md. A. B. H.; Yoo, M.; Nakamoto, H.; Watanabe, M. *Chem. Lett.* **2003**, *32*, 836.

(20) Belières, J. P. Protic Ionic Liquids, High Temperature Electrolytes for Fuel Cell Applications. Ph.D. Thesis, Arizona State University, 2005.

(21) Gurney, R. W. *Ionic processes in solution*; Dover Publications: New York, 1962; p 275.

(22) Yoshizawa, M.; Xu, W.; Angell, C. A. *J. Am. Chem. Soc.* **2003**, *125*, 15411.

(23) Belieres, J. P.; Angell, C. A. *J. Phys. Chem. B* **2007**, *111*, 4926.

(24) Kanzaki, R.; Uchida, K.; Song, X.; Umebayashi, Y.; Ishiguro, S.-I. *Anal. Sci.* **2008**, *24*, 1347.

(25) Kanzaki, R.; Uchida, K.; Hara, S.; Umebayashi, Y.; Ishiguro, S.-I.; Nomura, S. *Chem. Lett.* **2007**, *36*, 684.

(26) Fleischmann, M.; Hiddleston, J. N. *J. Sci. Instrum.* **1968**, *1*, 667.

(27) Barrette, W. C.; Sawyer, D. T. *Anal. Chem.* **1984**, *56*, 653.

(28) Varela, H.; Krischer, K. *Catal. Today* **2001**, *70*, 411.

(29) Fallis, S.; Anderson, G. K.; Rath, N. P. *Organometallics* **1991**, *10*, 3180.

(30) Reed, S. K.; Madden, P. A.; Papadopoulos, A. *J. Chem. Phys.* **2008**, *128*, 124701.

(31) Fedorov, M. V.; Kornyshev, A. A. *J. Phys Chem B* **2008**, *112*, 11868.

(32) Islam, Md. M.; Alam, M. T.; Ohsaka, T. *J. Phys. Chem. C* **2008**, *112*, 16568.

JP902762C